analytical chemistry

Article

Cite This: Anal. Chem. XXXX, XXX, XXX−XXX

pubs.acs.org/ac

Energy-Dispersive Total-Reflection Resonant Inelastic X-ray Scattering as a Tool for Elemental Speciation in Contaminated Water

José I. Robledo,*[,†,‡] Juan J. Leani,[†,‡] Andreas G. Karydas,[§,∥] Alessandro Migliori,[§] Carlos A. Pérez,[⊥] and Héctor J. Sánchez[†,‡]

[†]IFEG, National Scientific and Technical Research Council (CONICET), X5000HUA-Córdoba, Argentina

[‡]FaMAF, Universidad Nacional de Córdoba (UNC), X5000HUA-Córdoba, Argentina

[§]NSIL, International Atomic Energy Agency (IAEA), Friedensstrasse 1, A-2444 Seibersdorf, Austria

[∥]Institute of Nuclear and Particle Physics, NCSR "Demokritos", 153 10 Aghia Paraskevi, Athens Greece

[⊥]Brazilian Synchrotron Light Source (LNLS), CNPEM, 13083-970 - Campinas, Brazil

ABSTRACT: This work presents a state-of the-art analytical methodology, by which chemical state information on metallic elements is obtained for liquid samples in a fast and simple manner. This method overcomes limitations of conventional X-ray techniques, such as X-ray absorption spectroscopy, by applying resonant inelastic X-ray scattering under total reflection geometry (TRIXS). TRIXS is particularly applicable for the analysis of small quantity of liquid samples deposited on polished reflectors. This feature is relevant for the chemical speciation of metallic trace elements contained in water samples, since the degree of their toxicity depends crucially on the concentration of specific chemical species included. The analytical merits of the proposed methodology were studied at Elettra Sincrotrone Trieste and at the Brazilian Synchrotron Light Laboratory. Contaminated water samples with low concentration of different chromium and manganese compounds were measured. Results prove the analytical potential of the TRIXS technique in characterizing different chemical species of metallic elements in water samples.

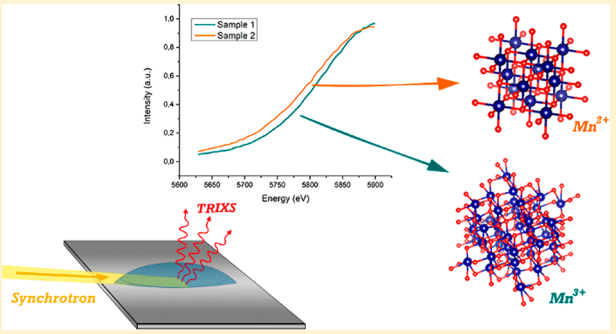

Water contamination can come from either natural or human sources. Anthropogenic causes include wastewater treatment effluent, landfill leachate, agricultural runoff, and a wide variety of industrial sources.

Heavy metals are among the most notorious water pollutants. These contaminants have been long detected as a threat to aquatic organisms and humans, even at trace concentrations.[1] They are known for their toxicity and persistence in the environment. Heavy metals have also the tendency to bioaccumulate in living tissues, reaching concentrations that can compromise the normal physiological processes of the absorbing organism, providing a potential pathway into the human food chain as well.[2] Several oligoelements, like lead, mercury or cadmium, are well-known hazardous pollutants. In some other cases, the chemical state of the metal can increase its toxicity, being arsenic the most notorious example.[3]

Chromium is a not very widespread case of an element commonly disposed by industries and factories; it has six species but only one of them is hazardous.[4] As chromium compounds are used in dyes and paints and in the tanning of leather, these compounds are often found in soil and groundwater at abandoned or even industrial sites, now needing environmental cleanup and remediation.[5] Another example of an industry demanding large amounts of chromium is that of primer paint, which contains hexavalent chromium, widely used for aerospace and automobile refinishing applications. Chromium commonly appears in nature as Cr(III) and Cr(VI), being the last one known for its toxicity.[6] There have been several attempts on discriminating these species of Cr in water and in soil by different methods,[7−9] with diverse levels of success.

Manganese is another example for which the association of the element's oxidation state regarding its toxicity is not carefully studied yet. Similar to the case of chromium, many compounds of Mn have an industrial use, for example, as divalent Mn acetate. They are used mainly in dyes or pigments or even as a catalyst, so different Mn compounds can be also found in soil and groundwater of industrial areas. It has been reported that the chronic exposure to manganese (Mn) produces deleterious effects on human health.[10] Some other experimental studies on animals have shown the effects of some chemical forms of Mn (as MMT and MnC12) on their health and behavior.[11]

Received: November 8, 2017
Accepted: February 7, 2018
Published: February 7, 2018

DOI: 10.1021/acs.analchem.7b04624
Anal. Chem. XXXX, XXX, XXX−XXX

Regarding the current regulations, the Environmental Protection Agency (EPA) of USA has defined a maximum contaminant level (MCL), as the highest level of a contaminant that is allowed in drinking water, of 0.1 mg/L for the total amount of Cr in water.[12] In the case of manganese, a Secondary MCL has been set in only 0.05 mg/L.[13]

It is clear that a simple and reliable tool for the proper discrimination, and characterization, of the different compounds of these metal contaminants is of the highest importance for both health and environmental science.

The aim of this work is to present a novel and different approach to the chemical speciation problem by presenting results on the determination of the chemical state and atomic environment of two contaminant elements, chromium and manganese, in dried water samples by means of resonant inelastic X-ray scattering in total reflection conditions, using an energy dispersive detection system. A multivariate statistical approach has been taken into account as to exploit the availability of such a rich data set, and to validate the proposed methodology.

X-ray Spectrochemical Technique. In the resonant inelastic X-ray scattering (RIXS) interaction, also known as X-ray resonant Raman scattering (RRS),[14] the scattered photons share an energy E_S with the emitted inner shell electrons of the irradiated atom, such that $E_S + T_e = E_0 - U_L$, where E_0 denotes the energy of the incoming photon, U_L the L-subshell binding energy of the target atom and T_e the kinetic energy of the corresponding L-subshell emitted electron. The energy sharing between the scattered RIXS photon and the emitted bound electron is based on the energy conservation between the initial and final states involved in the process. The RIXS spectrum shows a main peak structure centered around the maximum scattered photon energy $E_{S(max)} = E_0 - U_L$, namely, when the kinetic energy of the emitted electron is zero, but presenting a strong asymmetry at lower energies. The RIXS process generates a continuous energy spectrum, and in a similar manner as with the extended X-ray absorption fine structure (EXAFS) signal, it is expected for the emission spectrum to present small damped oscillations in the low energy side of the peak structure. Therefore, the analysis of the RIXS peak allows to establish a correspondence between the peak's oscillation pattern and the chemical state of the atom under study.[15] It should be noted that the possibility of characterizing the chemical environment of different elements in a variety of experimental conditions and samples, by means of RIXS spectroscopy, has been widely demonstrated in recent years.[16−18]

External total reflection is an inherent feature of X-rays resulting from the fact that, in the X-ray regime, the refractive index has a value for all materials slightly below one. Thus, the incoming X-rays can be totally reflected if the incident angle is less than a critical angle that takes values between one tenth of a degree, up to few degrees, depending on the reflector-material properties and the incoming X-ray energy. This feature offers also the possibility to perform optimum peak to background X-ray fluorescence (XRF) measurements under the external total reflection irradiation geometry (TXRF analysis), allowing the elemental analysis and characterization of trace and ultratrace quantities of particles and of dried residues deposited on smooth surfaces, such as silicon wafers.[19] Several papers have been published demonstrating the potentiality of external total reflection combined with different spectroscopic techniques, such as XRF,[20−23] EXAFS,[24,25] and even inelastic X-ray scattering (IXS) at grazing incidence conditions.[26,27] Applications of RIXS in total reflection geometry have been already reported using an energy dispersive system, showing a successful discrimination and characterization of arsenic species in water samples,[28] and of different chemical compounds contained in nanolayers.[29]

In the present work, the data set analyzed is a combination of measurements carried out in two different facilities, the IAEA end-station of the XRF beamline at the Elettra Sincrotrone Trieste, Italy, and the XRF D09B beamline at the Brazilian Synchrotron Light Source (LNLS). The sample sets studied in the present work consisted in a set of droplets with low concentration of Cr(III) and Cr(VI), and another set of droplets with low concentration Mn(II), Mn(IV), and Mn(VI) deposited on silicon wafers. Cr samples were of interest for addressing the environmental problem. Manganese samples were chosen because of the rich variety of oxidation states in the sample set, being suitable to show the methodology's potential and as a proof of concept in a different transition metal. After a minimum processing of the raw spectral data, a multivariate analysis was performed, involving principal component analysis (PCA), discriminant analysis (DA), and cross validation.

The results show patterns which are clearly correlated with the different Mn and Cr chemical compounds. The results of the present study suggest that the proposed analytical TRIXS methodology is a novel and reliable tool to perform chemical speciation analysis of toxic elements in contaminated water samples.

EXPERIMENTAL SECTION

Sample Description and Measurements. A total of six samples were prepared for these measurements. All of the samples consisted of 40 μL droplets, each of different solutions, dried on flat silicon wafers. These solutions consisted of different compounds in distilled water, with the metallic element of interest diluted to 1% by mass concentration.

Two of these samples were used to study chromium water contamination. The first solution (1) was made with chromium compound $CrCl_3$ (Cr^{3+}), while the second (2) was made with K_2CrO_4 (Cr^{6+}). The rest of the samples were prepared to study manganese water contamination. Sample 3 consisted of a solution of $MnCl_2{\cdot}(H_2O)$ (Mn^{2+}), sample 4 of $KMnO_4$ (Mn^{6+}), sample 5 of $Mn(H_2PO_2)_2$ (Mn^{2+}), and sample 6 of MnO_2 (Mn^{4+}). Since MnO_2 is not soluble in water, we studied a microgram quantity powder sample deposited directly onto a reflector, as to have a Mn^{4+} compound to enhance and to exploit the discriminant sensitivity of the multivariate analysis results. It is important to clarify that two samples of different chemical environments of Mn, but same oxidation state (Mn^{2+}), were chosen as to better comprehend the information given by the multivariate analysis.

The Mn samples measurements were carried out at Elettra Sincrotrone Trieste (EST, Italy) in the XRF beamline using the IAEA end station facility (IAEAXSpe).[30] This end-station consists of an ultrahigh vacuum chamber that includes a seven-axis motorized manipulator for sample and detectors positioning, different kinds of X-ray detectors and optical cameras. The detector used in this work was an ultrathin window Silicon Drift Detector (SDD) (Bruker, Germany) mounted in fixed position (90° in respect to the primary beam), with an energy resolution of ~131 eV for the Mn−Kα line. The flux of the primary X-ray beam was monitored by a diamond membrane

DOI: 10.1021/acs.analchem.7b04624
Anal. Chem. XXXX, XXX, XXX−XXX

detector (Dectris, Switzerland). A LabVIEW Graphical User Interface (GUI), designed and built by the NSIL group of the IAEA,[31] was utilized for data acquisition. The XRF beamline is equipped with a double crystal channel-cut monochromator, using a Si(111) crystal, having a resolving power of 1.4×10^{-4}. The incident beam had a size of approximately 250[h] × 120[v] microns at the sample position.

The Cr samples were measured at the Brazilian Synchrotron Light Laboratory (LNLS, Brazil) in the XRF station of the XRF-D09B beamline.[32] This beamline is equipped with a double-crystal "Channel-cut" monochromator based on a Si(111) crystal, resulting in a 3 eV energy resolution at 10 keV. The incident beam has a flux intensity on the sample of approximately 108 ph/s at 10 keV. For the measurements, a LEGe (Low Energy Germanium) solid-state detector was used with an energy resolution of 140 eV for the Mn−Kα line. The Minimum Detection Limit (MDL) of Fe for the TXRF technique of the station is 20 ppb.

For the TRIXS analysis of all samples, the irradiation geometry was arranged to fulfill the external total reflection condition, setting a grazing incidence angle for the exciting beam 0.1° below the respective critical angle, experimentally determined in an angular scan. Moreover, to benefit from the incident beam polarization at the electron orbit's plane, the detector axis was placed in the horizontal plane, thus minimizing the Compton and Rayleigh scattering.[33] The incident photon energy was set monochromatic, and its value was chosen to be 10 eV below the corresponding element's K-edge binding energy, that is, 6529 and 5979 eV for Mn and Cr respectively (as to enhance the RIXS intensity). Fifty spectrum repetitions were acquired for each Cr and Mn sample, resulting in a total of 100 spectra for the Cr samples and 200 for the Mn ones. The measuring time of each spectrum was set equal to 300 s.

TRIXS Spectra Analysis. A simple preprocessing of all measured spectra was required before performing any multivariate analysis. It consisted basically in two steps: (1) the separation of the region of interest (ROI) of the RIXS peaks from the rest of the spectrum (a region of 270 eV below the channel of maximum amplitude of the RIXS peak was used for both cases) and (2) the normalization of this ROI to its maximum amplitude value, leaving mainly the variability due to the oscillations present in the fine structure. Data profiles after preprocessing may be seen in Figures 1 and 2 for Mn and Cr set of samples respectively

A principal component analysis[34] (PCA) was first performed to both Mn and Cr spectra. PCA is an exploratory methodology that allows studying the variance and covariance structure of the measured variables (energy channels) throughout many measurements in a convenient way, by creating a linear combinations of them, and using just a few representative ones for the task. This technique allows a better comprehension of the underlying variability and covariability since it may drastically reduce the data set's dimension in the attempt to explain as much of the variance possible or of the variability of interest, without losing relevant information. This technique creates a new set of vectors, called the principal components (PC), which are linear combinations of the original variables, chosen in such a way as to maximize the variance they represent. From a mathematical point of view, suppose we have a set of p variables (energy channels) measured N times (total amount of spectra). If x_i (i = 1, ..., p) are the original variables, then we may choose the coefficients a_i of p new linear

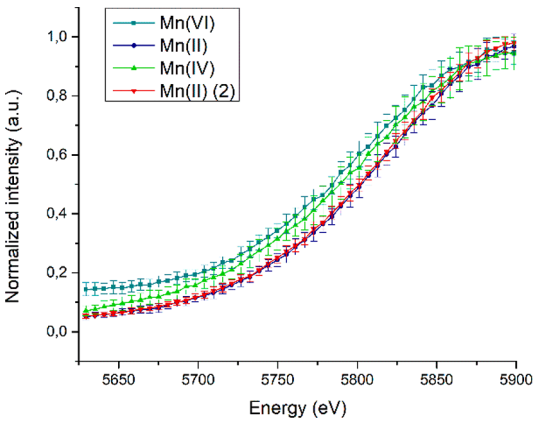

Figure 1. Energy region used for the PCA and DA procedures of Mn RIXS spectra (normalized to maximum amplitude). The average value of each energy channel over all measured spectra (for each of the samples) is shown. Error bars represent the standard deviation of the corresponding energy channel.

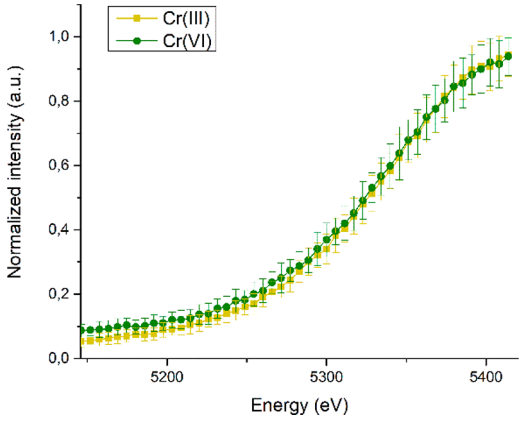

Figure 2. Energy region used for the PCA and DA procedures of Cr RIXS spectra (normalized to maximum amplitude). The average value of each energy channel over all measured spectra (for each of the samples) is shown. Error bars represent the standard deviation of the corresponding energy channel.

combinations $\boldsymbol{z}_i = \boldsymbol{a}_i \cdot \boldsymbol{X}$ (where $\boldsymbol{X}$ is the $N \times p$ matrix of the data) as to maximize its variance. This means that we are looking for

$$\max[\mathrm{var}(\mathbf{z}_i)] = \max[\mathbf{a}_i^T \Sigma \mathbf{a}_i], \quad \text{for } i = 1, \ldots, p$$

where $\sum$ is the covariance matrix of the data set. If we define the variance of the linear combination z_i as $\lambda = \frac{\mathrm{var}(\mathbf{z})}{|a|} = \frac{a^T \Sigma a}{a^T a}$, then obtaining the maximum value of λ is equivalent to solving the eigenvalue equation $(\sum - \lambda_i \boldsymbol{I}) \cdot \boldsymbol{a}_i = 0$ for the covariance matrix and selecting the largest eigenvalue. The principal component 1 (PC1) is defined as the eigenvector corresponding to the largest eigenvalue, PC2 is defined as the eigenvector corresponding to the second largest eigenvalue, and so on. Since eigenvectors are orthogonal, each PC explains different parts of the total variability, and it is easy to see that the total variability is obtained by summing the variance explained by each of the PC. From a geometrical point of view, performing a PCA to a data set is equivalent to obtaining a set of new axes in the p dimensional space that consist on centering the original axes on the data cloud, and rotating them as to align them with the axes of maximum variance in it.

DOI: 10.1021/acs.analchem.7b04624
Anal. Chem. XXXX, XXX, XXX−XXX

In order to objectively compare the oscillation patterns present in the RIXS spectra, a linear discriminant analysis (LDA) was performed. This technique is especially relevant in the Mn case since this data set presents more than two classifying labels, allowing the observation of the variability in a plane. LDA is a multivariate technique which is widely used for classification. It is especially useful when one has previous knowledge of the category of some of the samples to be discriminated because it uses this information as to classify the rest. This technique searches the p-dimensional space in the attempt to find the most discriminant set of vectors with respect to the selected categories. The idea is to map the high dimensional data set onto a lower-dimensional space which allows the best discrimination. This lower dimensional space is obtained by the set of most discriminant projection vectors found by the LDA. In this space, all projected samples will form the maximum between-class scatter and the minimum within-class scatter simultaneously. This idea belongs to Fisher[35] and it is sometimes called as Fisher's discriminant analysis. Mathematically speaking, the variability *between* classes may be written as

$$b(\mathbf{e}) = \sum_{\alpha=1}^{N} |\mathbf{e}^T(\boldsymbol{\mu}_\alpha - \bar{\boldsymbol{\mu}})|^2$$

where N is the number of classes in the data set (two for Cr and three for Mn), $\boldsymbol{e}$ is a vector pointing in some particular direction, $\boldsymbol{\mu}_\alpha$ the mean of the random vectors $\boldsymbol{x}_\alpha$ (in our case the mean of the spectra of one class), and $\bar{\boldsymbol{\mu}}$ the mean vector of the N vectors $\boldsymbol{\mu}_\alpha$. Following the same notation, the variability *within* a class may be written as

$$w(\mathbf{e}) = \sum_{\alpha=1}^{N} \mathrm{var}(\mathbf{e}^T\mathbf{x}_\alpha)$$

So, the idea of Fisher's Discriminant Analysis is to find $\boldsymbol{e}$ so as to maximize the ratio:

$$\delta = \max\left(\frac{b(e)}{w(e)}\right)$$

If we obtain the matrices B and W that satisfy that $b(\boldsymbol{e}) = \boldsymbol{e}^T B\boldsymbol{e}$ and $w(\boldsymbol{e})$ $\boldsymbol{e}^T W\boldsymbol{e}$, then it is possible to obtain the direction $\boldsymbol{e}$ that maximizes the value of δ in the same way as in PCA, but by Eigen decomposition of the matrix $W^{1-}B$ instead of $\sum$ (the covariance matrix).

As to estimate our technique's predictive capability, a k-fold cross validation (CV) was performed for each data set ($k = 2$ for Cr and $k = 4$ for Mn).[36] In this type of CV, the data set is randomly split into k mutually exclusive subsets (the folds) of approximately equal size. As to understand this estimation method, we briefly define some keywords and reference them to our data set. A *classifier* is a function that maps an *unlabeled instance* (a spectrum of a sample with unknown oxidation state) to a *label* (the oxidation state, e.g. Cr(III) or Cr(VI)) using internal data structures (the correlations in the oscillations). An *inducer* (also called *induction algorithm*) builds a classifier from a given data set. In our case, the inducer is the LDA or PCA performed on each fold, and the classifier is the canonical axis or principal component obtained respectively (some specific linear combination of the spectrum's energy channels). The *accuracy* of our classifier is the probability of correctly classifying a randomly selected spectra. If X is the total data set, then in each fold it is divided into two subsets, X_t and $X|X_t$, where the first is called the testing subset, and the latter the training subset (the leftover spectra). The inducer is trained and tested k times. This means that, in each $t \in \{1, 2, ..., k\}$, the inducer is trained in $X|X_t$ and tested in X_t. For each fold, the estimate of accuracy is obtained as the total number of correct classifications divided by the number of spectra in the data set. For the k-fold CV, the *cross-validation estimate of accuracy* is the average of the estimates of accuracy on each fold.

RESULTS AND DISCUSSION

Figures 1 and 2 show the region used for the PCA and DA procedures for Mn and Cr samples, respectively. All the spectra were normalized to the maximum amplitude of the RIXS peak. Since several RIXS spectra were recorded for each sample, the above-mentioned figures display, for each sample, the mean value and standard deviation of each channel content within the region of interest.

As it can be seen, it is impossible, a priori, to properly discriminate the different species. Nevertheless, it is possible to observe in Figure 3 how the Principal Component Analysis finds an adequate plane in which the spectra belonging to the Cr(III) and Cr(VI) samples are clearly differentiated. For clarity, we remind the reader that each point in the PC1−PC2 plane represents a measured spectra. The position they have in this plane is the calculated value of both principal component functions, taking its energy channels as input values. It is important to understand that the only channels used were the normalized ones belonging to the RIXS region, where the dampened oscillations are present. What is nonobservable by a visual inspection of Figure 2 is being completely noticed by the analysis.

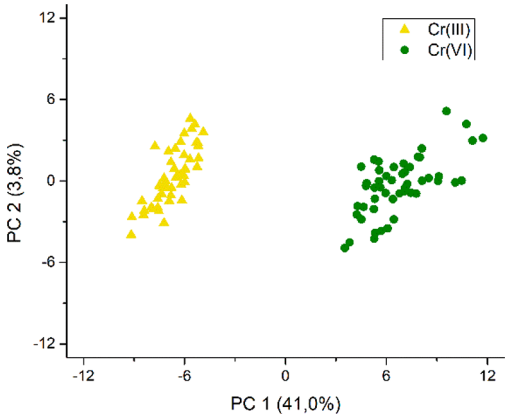

Figure 3. Projection of the chromium data cloud onto principal components 1 and 2. The measured spectra from the Cr(III) sample are represented with yellow triangles and the ones from the Cr(VI) sample in green dots.

The PCA's result for the Mn data set is shown in Figure 4. This figure shows the projections of every measured Mn spectra onto the PC1−PC2 plane. The percentage given in parentheses is the amount of the total variance explained by the corresponding principal component. Taking into account both PC1 and PC2, a 50.54% of the total variance is visualized in this plane. However, only the 35.24% variance from the data set explained by the PC1 is required to discriminate the different Mn oxidation states. It should be noticed that, as PC's are orthogonal, the variability shown by one PC is not observable in the rest of the PC's. Therefore, by observing the

DOI: 10.1021/acs.analchem.7b04624
Anal. Chem. XXXX, XXX, XXX−XXX

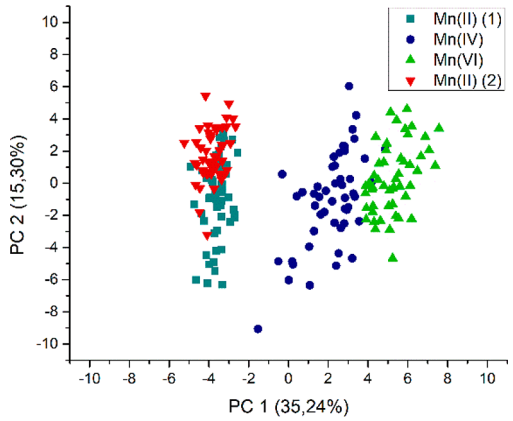

Figure 4. Projection of the manganese data cloud onto principal components 1 and 2 axes.

projection onto the PC1−PC2 plane we are missing a 49.46% of the total variability in the data set. Even so, this missing variability shows to be unnecessary for our discrimination task. To comprehend this last point, it should be observed that the principal component 1 is enough to discriminate the Mn(II) spectra (with a centroid of the data cloud around PC1 = −4) from the Mn(IV) spectra (centroid around PC1 = 2), and from the Mn(VI) measurements (centroid around PC1 = 6). This is achieved just by studying a 35.24% of the total variability.

Exploratory results, as the ones obtained above, are really interesting and allow to infer the underlying structure from the clustering of spectra of the same species in the PC1−PC2 plane. There is a correlation between the element's species and the spatial distribution in this specific projection plane (in fact, it suffices to only observe the PC1 axis). But sometimes, like in the Mn case, it is possible to take it another step forward. We may use the fact of having TRIXS spectra of two Mn chemical compounds, but with the same Mn oxidation state. We may also contemplate in our analysis the fact that we have three different classes, something that is not contemplated at all when performing a PCA. This "extra" information is taken into account by the linear discriminant analysis. Figure 5 shows the results of a 4-fold cross validation (CV) performed to the data

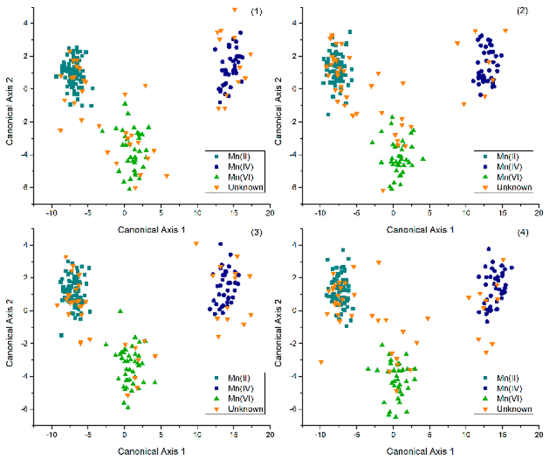

Figure 5. 4-Fold cross-validation in DA of manganese data set. In each of the four groups, a set of 50 spectra have been randomly removed (and labeled as "unknown"), and for each group, the canonical axes have been calculated with the rest. Afterward, the unknown spectra are evaluated and plotted.

set as to show the LDA efficiency to discriminate Mn compounds. In each of these CVs, a random set of 50 spectra were separated from the total set of 200 spectra. The 150 leftovers were used to create the canonical axes (through the LDA) and with these new canonical axes, the 50 "unknown" samples were classified in the possible categories (Mn(II), Mn(IV), or Mn(VI)). For each spectrum, the classification obtained by the LDA was compared to its known oxidation state as to establish an error measurement for the classification.

In all four cross validations shown in Figure 5, the accuracy of the LDA was of 100%, meaning that every spectrum was correctly classified with respect to its oxidation state. The results of this 4-fold CV gives a statistical sustain to the classification ability of our technique.

We also performed a simple cross validation to the PCA results of the Mn data set. We left out of the PCA all spectra belonging to one of the Mn(II) samples, and performed the analysis with the rest of the spectra. Afterward, we evaluated PC1 and PC2 for the left out spectra and plotted every spectra in the PC1−PC2 plane. This was performed two times, each time leaving out one of the two Mn(II) samples. Figure 6

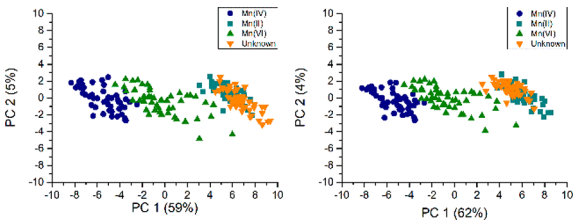

Figure 6. Cross validation in PCA for Mn(II) data.

shows the results obtained in both cases. It is possible to see that in both CV's, the PC1 obtained by the PCA is equally discriminative and that the result is independent of which Mn(II) compound was selected to perform the analysis.

The presented results clearly support the discrimination capability of this methodology (See Figures 3 and 4). The cross-validation results show that the principal components and canonical axes generated with the different methods do not depend on the specific data set used for their generation, rather depend on the existing internal structure of the oscillations. They also show that these generated functions work as good predictors for a set of unknown spectra, since they resulted in 100% accuracy when classifying.

This technique may present some potential drawbacks when analyzing complex samples with many elements of similar atomic number. This problem can be solved by selecting a smaller ROI for the RIXS tail. Most of the times, this procedure is sufficient to continue with a correct analysis.

The analysis here performed contemplates the excitation of a K-shell electron. Nevertheless, this analysis can also be applied to L (and even M) lines by setting the incident energy under an L (or M) absorption edge. This could give sensitive information about the electron configuration, providing complementary information to the analysis performed on the K edge, broadening the reach of this methodology, and allowing the study of heavy elements as well.

CONCLUSIONS

This work shows the potentiality of energy dispersive RIXS spectroscopy applied under external total reflection sample irradiation geometry, combined with multivariate analysis tools

DOI: 10.1021/acs.analchem.7b04624
Anal. Chem. XXXX, XXX, XXX−XXX

(principal component analysis (PCA) and linear discriminant analysis (LDA)) to characterize different chemical species of metals in contaminated water samples. This outcome has been validated by complementary Cross Validation (CV) procedures. Due to the versatility of the RIXS methodology, the different experimental XRF setup configurations (such as grazing incidence, grazing exit, confocal, etc.) can be also used for depth resolved chemical speciation analysis from the nm to sub-millimeter range. The proposed analytical methodology can be applied even in a conventional X-ray laboratory by utilizing an X-ray tube in conjunction with an appropriate secondary stage (equipped with a fluorescent target/filter or diffractive crystal) to produce a highly monochromatic exciting beam, avoiding the need of visiting a synchrotron radiation facility.

AUTHOR INFORMATION

Corresponding Author

*E-mail: jorobledo@unc.edu.ar.

ORCID

José I. Robledo: 0000-0001-8784-2558

Author Contributions

The manuscript was written through contributions of all authors. All authors have given approval to the final version of the manuscript.

Notes

The authors declare no competing financial interest.

ACKNOWLEDGMENTS

The authors would like to acknowledge the financial support of the International Atomic Energy Agency (IAEA) through the CRP No. 18182, and the support of the Brazilian Synchrotron Light Laboratory (LNLS) through project number XAFS1-17082. The authors would also like to thank Dr. Mónica Balzarini for her helpful comments on the statistical procedure.

REFERENCES

(1) Tchounwou, P. B.; Yedjou, C. G.; Patlolla, A. K.; Sutton, D. J. *EXS* **2012**, *101*, 133−164.
(2) du Preez, H. H.; Steyn, G. J. *Water SA* **1992**, *18*, 131−136.
(3) Duffus, J. H. *Pure Appl. Chem.* **2002**, *74* (5), 793−807.
(4) Kotaś, J.; Stasicka, Z. *Environ. Pollut.* **2000**, *107* (3), 263−283.
(5) Matteoda, E.; Blarasin, M.; Damilano, G.; Cabrera, A.; Giuli-ano Albo. *J. Bol. Geológico Min.* **2010**, *120* (4), 617−630.
(6) Shanker, A.; Cervantes, C.; Lozatavera, H.; Avudainayagam, S. *Environ. Int.* **2005**, *31* (5), 739−753.
(7) Inui, T.; Abe, W.; Kitano, M.; Nakamura, T. *X-Ray Spectrom.* **2011**, *40* (4), 301−305.
(8) Aranda, P. R.; Moyano, S.; Martinez, L. D.; De Vito, I. E. *Anal. Bioanal. Chem.* **2010**, *398* (2), 1043−1048.
(9) Liu, X.; Li, T.; Wu, Q.; Yan, X.; Wu, C.; Chen, X.; Zhang, G. *Talanta* **2017**, *165*, 216−222.
(10) Barbeau, A. *NeuroToxicology* **1994**, *5*, 13−36.
(11) Fishman, B.; McGinley, P. A.; Gianutsos, G. *Toxicology* **1987**, *45*, 193−201.
(12) United States Environmental Protection Agency. National Primary Drinking Regulations, 2017. https://www.epa.gov/ground-water-and-drinking-water/national-primary-drinking-water-regulations#one.
(13) United States Environmental Protection Agency. Secondary Drinking Water Standards, 2017. https://www.epa.gov/dwstandardsregulations/secondary-drinking-water-standards-guidance-nuisance-chemicals.
(14) Sparks, C. J., Jr. *Phys. Rev. Lett.* **1974**, *33*, 262−265.
(15) Leani, J. J.; Sánchez, H. J.; Valentinuzzi, M. C.; Pérez, C. A. *J. Anal. At. Spectrom.* **2011**, *26*, 378−382.
(16) Leani, J. J.; Sanchez, H. J.; Valentinuzzi, M. C.; Pérez, C. A. *X-Ray Spectrom.* **2011**, *40*, 254−256.
(17) Leani, J. J.; Sánchez, H. J.; Pérez, D.; Pérez, C. *Anal. Chem.* **2013**, *85*, 7069.
(18) Robledo, J. I.; Sánchez, H. J.; Leani, J. J.; Pérez, C. *Anal. Chem.* **2015**, *87*, 3639.
(19) Klockenkämper, R. *Total Reflection X-ray Fluorescence Analysis*; John Wiley & Sons, Inc.: New York, 1997.
(20) Iida, A.; Yoshinaga, A.; Sakurai, K.; Gohshi, Y. *Anal. Chem.* **1986**, *58*, 394.
(21) Vazquez, C.; Boeykens, S.; Elkin, D. *Technical Briefs in Historical Archaeology* **2010**, *5*, 10.
(22) Prange, A. *Spectrochim. Acta, Part B* **1989**, *44*, 437.
(23) Klockenkamper, R.; von Bohlen, A. *J. Anal. At. Spectrom.* **1992**, *7*, 273.
(24) Barchewitz, R.; Cremonese-Visicato, M.; Onori, G. *J. Phys. C: Solid State Phys.* **1978**, *11*, 4439.
(25) Barrett, N. T.; Gibson, P. N.; Greaves, G. N.; Mackle, P.; Roberts, K. J.; Sacchi, M. *J. Phys. D: Appl. Phys.* **1989**, *22*, 542.
(26) Murphy, B. M.; Müller, M.; Stettner, J.; Requardt, H.; Serrano, J.; Krisch, M.; Press, W. *J. Phys.: Condens. Matter* **2008**, *20*, 224001.
(27) Fister, T. T.; Fong, D. D.; Eastman, J. A.; Iddir, H.; Zapol, P.; Fuoss, P. H.; et al. *Phys. Rev. Lett.* **2011**, *106*, 037401.
(28) Sánchez, H. J.; Leani, J. J.; Pérez, R. D.; Pérez, C. *J. Appl. Spectrosc.* **2013**, *80*, 920−924.
(29) Leani, J. J.; Sánchez, H. J.; Pérez, C. *J. Spectrosc.* **2015**, *2015*, 618279.
(30) Karydas, A. G.; Czyzycki, M.; Leani, J. J.; Migliori, A.; Osan, J.; Bogovac, M.; Wrobel, P.; Vakula, N.; Padilla-Alvarez, R.; Menk, R. H.; et al. *J. Synchrotron Radiat.* **2018**, *25* (1), 189−203.
(31) Wrobel, P.; Bogovac, M.; Sghaier, H.; Leani, J. J.; Migliori, A.; Padilla-Alvarez, R.; Czyzycki, M.; Osan, J.; Kaiser, R. B.; Karydas, A. G. *Nucl. Instrum. Methods Phys. Res., Sect. A* **2016**, *833*, 105.
(32) Pérez, C. A.; Radtke, M.; Sánchez, H. J.; Tolentino, H.; Neuenshwander, R. T.; Barg, W.; Rubio, M.; Silveira Bueno, M. I.; Raimundo, I. M.; Rohwedder, J. R. *X-Ray Spectrom.* **1999**, *28*, 320.
(33) Hanson, A. L. *Nucl. Instrum. Methods Phys. Res., Sect. A* **1986**, *243*, 583−598.
(34) Johnson, R. A.; Wichern, D. W. In *Applied Multivariate Statistical Analysis*; Prentice Hall, Inc., 1992.
(35) Fisher, R. A. *Annals of eugenics* **1936**, *7* (2), 179−188.
(36) Kohavi, R. *Proceedings of the Fourteenth International Joint Conference on Artificial Intelligence* **1995**, *2* (12), 1137−1143.

DOI: 10.1021/acs.analchem.7b04624
Anal. Chem. XXXX, XXX, XXX−XXX